Supporting information

Enhanced Activity towards Oxygen Electrocatalysis for Rechargeable Zn-Air Batteries by Alloying Fe and Co in N-Doped Carbon

*Fengjiao Yu, Qi Ying, Shaofeng Ni, Chenxue Li, Daxiang Xue and Yang Yang**

State Key Laboratory of Materials-Oriented Chemical Engineering, College of Chemical Engineering, Nanjing Tech University, Nanjing 211816, China

*Corresponding Author; Email: yangy@njtech.edu.cn

Experimental

Materials

All reagents and chemicals were of analytical grade and used without further purification. $Co(AC)_2 \cdot 4H_2O$ (99%, AR), $Fe(NO_3)_3 \cdot 9H_2O$ (99%, AR), NH_4Cl (99%, AR) and glucose (99%, AR) were purchased from Sinopharm Chemical Reagent. HCl (98%), potassium hydroxide and dicyandiamide were obtained from Shanghai Lingfeng Reagent. Nafion (5 wt%) was obtained from Aldrich. Commercial Pt/C (20 *wt.%*) was obtained from Johnson Matthey Chemicals Ltd. and RuO_2 (99.9%) was purchased from Aladdin Industrial Corporation.

Synthesis of FeCo/N-C, Fe/N-C and Co/N-C

The typical synthetic process was as follows: 2 g of dicyandiamide, 10 g of ammonium chloride, 0.15 mmol of $Co(Ac)_2 \cdot 4H_2O$ and 0.15 mmol of $Fe(NO_3)_3 \cdot 9H_2O$ were dissolved in 200 mL deionized water, followed by freeze-drying. Then 4 g of freeze-dried powder was placed in a crucible and heated at 450^{o}C for 2 h with a rate of 2^{o}C/min from room temperature to 450 ^{o}C.

For the synthesis of FeCo/N-C, 0.5 g FeCo-doped *g*-C_3N_4 was dispersed in 35 mL of 0.03 M glucose solution under sonication for 2 h. Then the above mixture was heated at 90 ^{o}C for 12 h to get dry powder. For the calcination process, the powder was annealed at 450 ^{o}C for 1 h at a speed of 2 ^{o}C/min, followed by 850 ^{o}C for 2 h at a speed of 8 ^{o}C/min under N_2 atmosphere. After cooling down, the carbonized products were soaked with hydrochloric acid (1 M) overnight, washed by deionized water several times and dried at 80 ^{o}C overnight. The as-prepared sample was named as FeCo/N-C (Fe_5Co_5-NC). Fe/N-C or Co/N-C samples were prepared with merely addition of Co or Fe precursors.

We also varied the ratio of Fe and Co precursors for optimization. The FeCo/N-C sample has a precursor molar ratio of Fe:Co = 5:5. FeCo 2:8 and FeCo 8:2 were prepared by the same procedure with different molar ratios but constant metal content.

Characterizations

Scanning electron microscopy (SEM) was performed on a Hitachi S-4800 microscope. X-ray diffraction (XRD) measurements were conducted from 5^o to 80^o at a scan rate of

0.2^{o}/s on an intelligent laboratory diffractometer (Rigaku Inc.). Transmission electron microscopy (TEM) and high resolution transmission electron microscopy (HRTEM) studies were performed on a JEOL 2100 Plus microscope at 200 kV. The TEM microscopes are equipped with energy dispersive X-ray spectrometers (EDX) for elemental analysis. X-ray photoelectron spectroscopy (XPS) spectra were obtained by Thermo 250XI instrument. The Raman spectra were collected on a Labram HR Evolution instrument with a wavelength range from 500 to 2000 cm^{-1}.

Electrochemical Measurements

For preparation of working electrode, 2 mg of electrocatalyst samples was dispersed in a mixed solution containing 380 μL anhydrous ethanol, 20 μL Nafion and 100 μL deionized water, and under ultrasonic for 2 h until a uniformly dispersed black suspension was formed. Then 16 μL of the ink was dropped on the surface of a rotating disc electrode (RDE) with a final loading density of 0.326 mg/cm^2. The resulting electrode served as the working electrode.

The electrocatalytic performance of the samples was tested on a workstation (Ivium-n-Stat) equipped with a high-speed rotator at room temperature. The RDE as the working electrode, graphite rod as the counter electrode and Ag/AgCl electrode (3.5 M KCl) as the reference electrode, compose a three-electrode test system. And the electrolyte solution is KOH. The potentials were converted to RHE according to the following formula: $E_{RHE} = E_{Ag/AgCl} + 0.059 \cdot pH + E^{\ominus}_{Ag/AgCl}$.

The linear sweep voltammetry (LSV) measurement was performed in the voltage range from 0.2 V to 1.2 V vs. RHE for ORR and from 0.9 V to 1.8 V vs. RHE for OER. The working electrode scanned the LSV curves in KOH solution saturated with O_2 at different speeds (900, 1225, 1600, 2025 and 2500 rpm) with a scan rate of 5 mV/s. The electron transfer number (n) can be calculated through the following Koutecky-Levich (K-L) equations:

$$\frac{1}{j} = \frac{1}{j_L} + \frac{1}{j_K} = \frac{1}{B\omega^{1/2}} \quad (1)$$

$$B = 0.62\mathrm{n}FC_{O_2}(D_{O_2})^{2/3}V^{-1/6} \quad (2)$$

where, J is the measured current density, J_K is the kinetic current density, and J_L is the limiting diffusion current density, ω is the rotating speed of the rotating disc electrode, rpm, n is the electron transfer number, F is Faraday constant, 96485 C/mol, C_{O2} is the oxygen concentration in an oxygen-saturated 0.1 M KOH solution, 1.2×10^{-3} mol/L, D_{O2} is the diffusion coefficient of oxygen in 0.1 M KOH solution saturated with oxygen, 1.9×10^{-3} cm^2/s, The v is the kinematic viscosity coefficient of oxygen saturated 0.1 M KOH solution, 1.2×10^{-3} cm^2/s.

The tolerance of methanol was tested by chronocurrent method (*I-t*) at a voltage of 0.6V vs. RHE, with addition of 1 M methanol at 300 s.

Zn-Air Battery Tests

The air cathode was prepared by loading the synthesized sample on carbon paper with a weight of 1 mg/cm^2. The zinc plate was used as anode and 6 M KOH solution containing 0.2 M $ZnCl_2$ was used as the electrolyte. The charge–discharge cycling test was carried out at room temperature, with the current density of 10 mA/cm^2, and each period of 10 min.

Figures

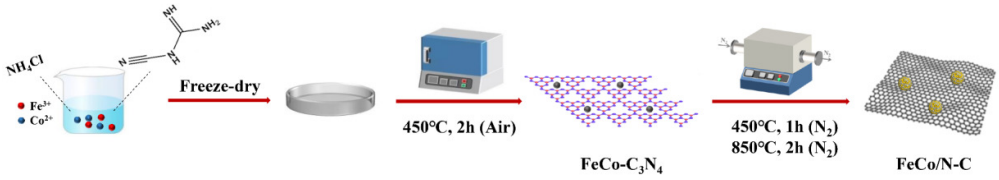

Scheme S1. Illustration of the two-step synthesis of the FeCo/N-C catalyst.

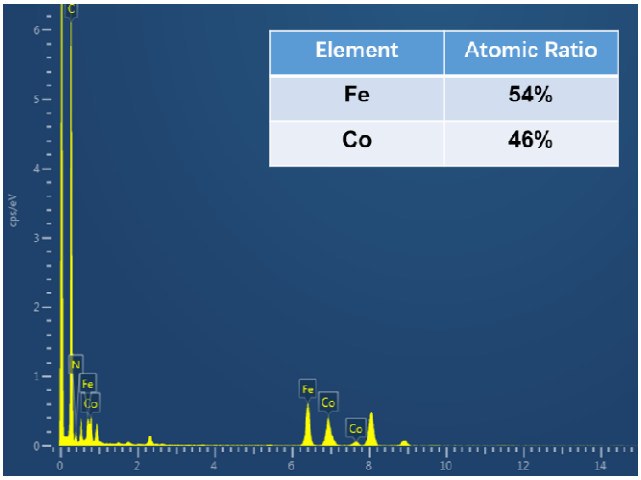

Figure S1. EDX spectrum of FeCo/N-C sample with inset showing the atomic ratio of Fe and Co elements.

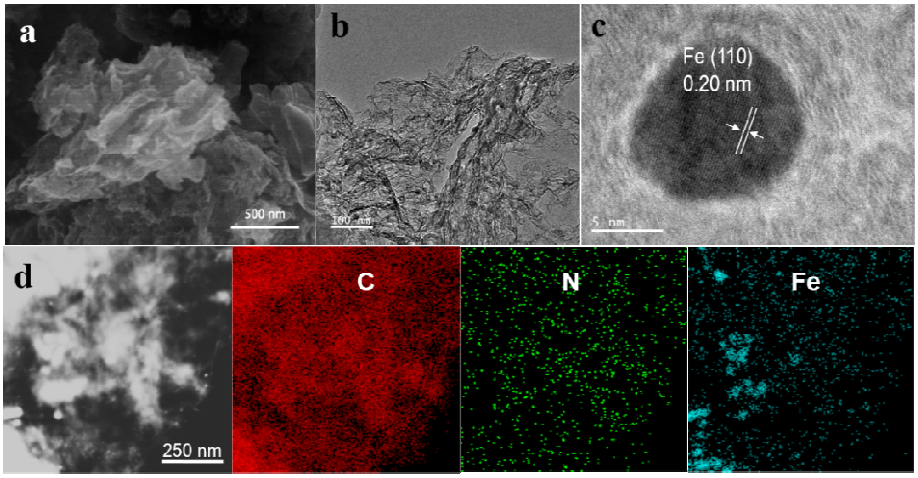

Figure S2. (a) SEM and (b) low-magnification TEM images of Fe/N-C. (c) HRTEM image of one Fe nanoparticle embedded in the carbon layers. (d) HAADF image and elemental mappings of C, N and Fe.

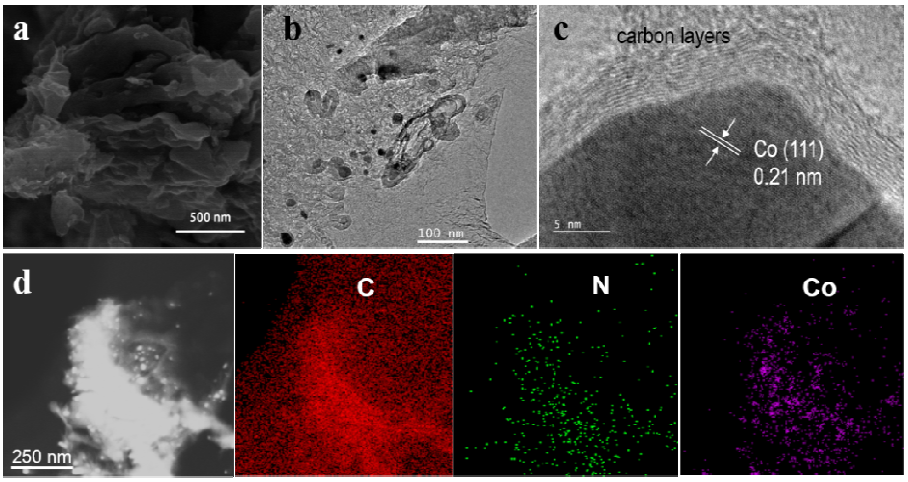

Figure S3. (a) SEM and (b) low-magnification TEM images of Co/N-C. (c) HRTEM image of one Co nanoparticle embedded in the carbon layers. (d) HAADF image and elemental mappings of C, N and Co.

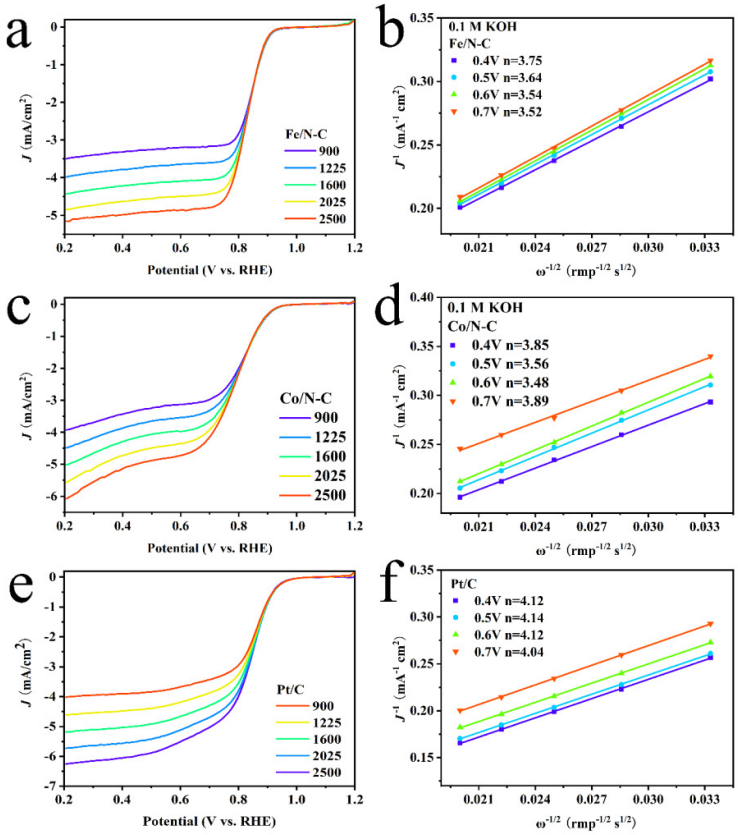

Figure S4. (a, c, e) LSV polarization curves at various rotation speeds in 0.1 M KOH and (b, d, f) the respective K–L plots at diverse potentials for Fe/N-C, Co/N-C and Pt/C.

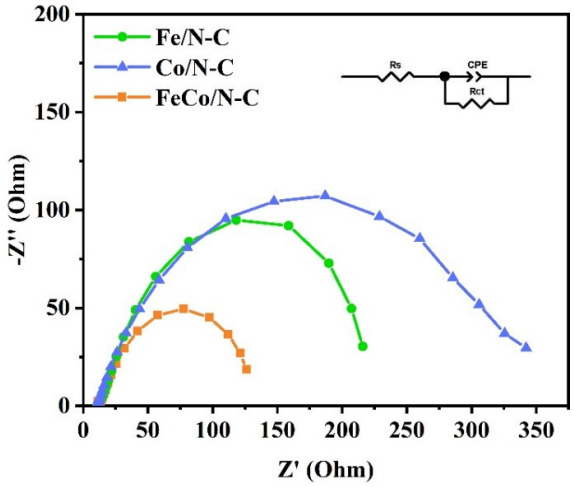

Figure S5. EIS spectra and equivalent circuit diagram of Fe/N-C, Co/N-C and FeCo/N-C.

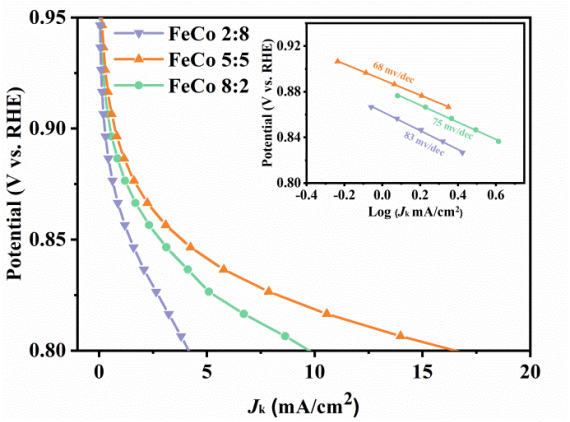

Figure S6. ORR specific kinetic current densities (J_k) and corresponding Tafel plots of FeCo 2:8, 5:5 and 8:2 catalysts (inset).

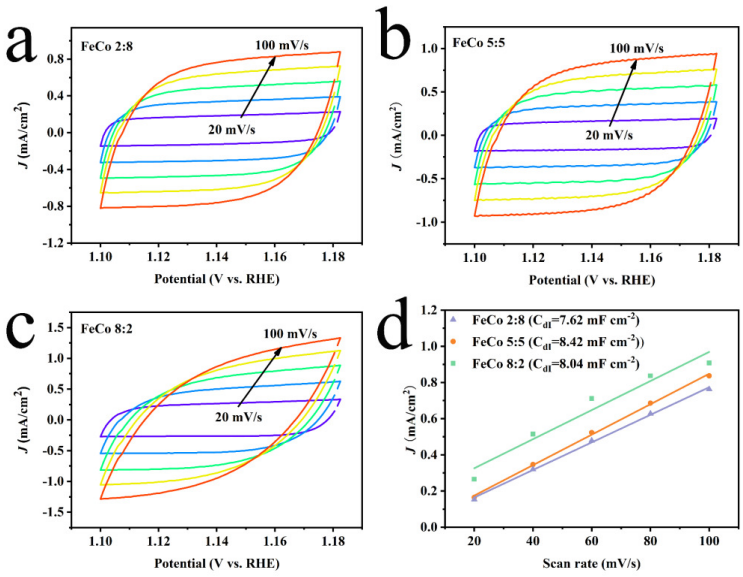

Figure S7. CV plots with different scan rates in 0.1 M KOH solution for (a) FeCo 2:8, (b) 5:5 and (c) 8:2 catalysts. (d) Current densities as a function of the scan rate for the examined catalysts showing the Cdl values of the three samples.

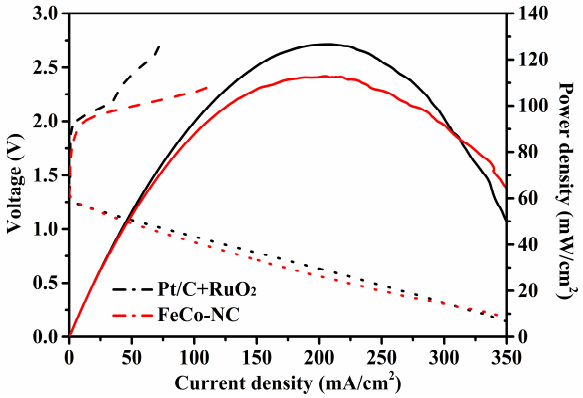

Figure S8. Charge and discharge polarization curves and corresponding power density curves of the Zn-air batteries with Pt/C+RuO_2 and FeCo/NC as the air cathode catalysts.

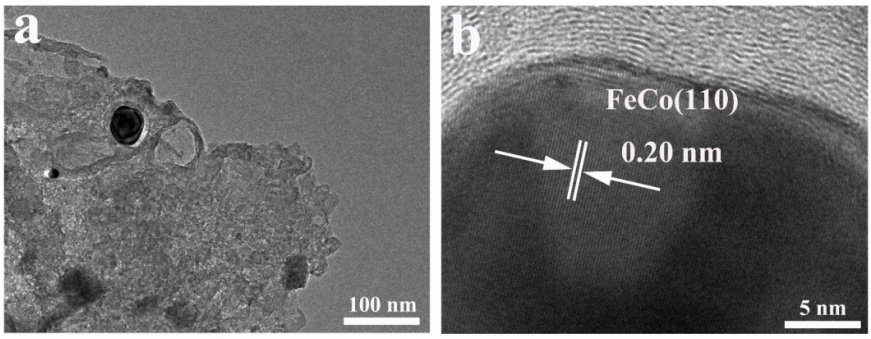

Figure S9. TEM images of FeCo/N-C catalyst after cycling test in Zn-air battery and the lattice fringes can be indexed to FeCo (110) planes.

Table S1. Summary of the performance of reported transition-metal based bifunctional catalysts.

Electrocatalyst	$E_{1/2}$ (V vs. RHE)	E_{10} (V vs. RHE)	ΔE (V)	Tafel slope (mV dec^{-1}) ORR	Tafel slope (mV dec^{-1}) OER	Loading (mg/cm^2)	Electrolyte KOH	Reference
FeCo/N-C	0.84	1.575	0.735	68	88	0.33	ORR: 0.1 M KOH; OER: 1 M KOH	this work
Fe/N-C	0.82	1.647	0.827	70	102	0.33	ORR: 0.1 M KOH; OER: 1 M KOH	this work
Co/N-C	0.79	1.677	0.887	102	99	0.33	ORR: 0.1 M KOH; OER: 1 M KOH	this work
Fe–N–C/ NiFe-LDH	0.792	1.539	0.747	/	/	0.2	0.1 M KOH	[1]
FeCo–N–C-700	0.896	1.6	0.704	87	72	0.4	0.1 M KOH	[2]
$Fe_{0.5}Co_{0.5}O_x$/NrGO	0.747	1.487	0.74	62.2	30.1	0.5	0.1 M KOH	[3]
FePc-GO	0.89	1.65	0.76	/	112	0.2	0.1 M KOH	[4]
$CoFe_2O_4$	0.73	1.64	0.91	53	/	0.15	0.1 M KOH	[5]
$NiFe_2O_4$	0.68	1.64	0.96	57	/	0.15	0.1 M KOH	[5]
Ni_3FeN/NRGO	0.7	1.63	0.93	/	/	0.1	0.1 M KOH	[6]
$FeCo_{(a)}$-ACM	0.9	1.6	0.7	79.73	261.2	0.4	ORR: 0.1 M KOH; OER: 1 M KOH	[7]
FeCo-NGS-800	0.84	1.61	0.77	102.5	108.2	0.2	ORR: 0.1 M KOH; OER: 1 M KOH	[8]
$Co_{0.5}Fe_{0.5}S$@N-MC	0.81	1.64	0.83	67	159	0.8	ORR: 0.1 M KOH; OER: 1 M KOH	[9]
Mn/Co-N-C	0.8	1.66	0.86	77	145	0.25	0.1 M KOH	[10]
$NiCo_2S_4$ HSs	0.8	1.63	0.83	48.6	93.7	0.5	0.1 M KOH	[11]
$Co_3FeS_{1.5}(OH)_6$	0.721	1.588	0.867	96	79	0.25	0.1 M KOH	[12]
Co-Ni-S@NSPC	0.82	1.7	0.88	/	114	0.39	0.1 M KOH	[13]
$NiCoO_2$/CNTs	0.67	1.66	0.99	/	156	0.51	0.1 M KOH	[14]
CoFe/N-GCT	0.79	1.67	0.88	71	106	0.597	0.1 M KOH	[15]
FeCo/N-DNC	0.81	1.62	0.81	/	68	0.102	0.1 M KOH	[16]

Table S2. Comparison of the performance of Zinc-air batteries of FeCo/N-C and other reported catalysts.

Electrocatalyst	power density ($mW\ cm^{-2}$)	Loading (mg/cm^2)	Note	Reference
FeCo/N-C	112.7	1		this work
$CoSe_2$-NCNT NSA	51.1	-	flexible battery	[17]
Co-SAs@NC	105.3	1.75		[18]
Ni–Co–S/NSC	137	2		[19]
CoNi-SAs/NC	101.4	1.4		[20]
MnO/Co/PGC	172	10		[21]
CoS_x/Co-NC-800	103	1		[22]
CoNMC-700-1	69.6	1		[23]
S-GNS/$NiCo_2S_4$	216	0.42		[24]

[1] S. Dresp, F. Luo, R. Schmack, S. Kuehl, M. Gliech, P. Strasser, *Energy Environ. Sci.* **2016**, *9*, 2020.

[2] X. Duan, S. Ren, N. Pan, M. Zhang, H. Zheng, *J. Mater. Chem. A* **2020**, *8*, 9355.

[3] L. Wei, H. E. Karahan, S. Zhai, H. Liu, X. Chen, Z. Zhou, Y. Lei, Z. Liu, Y. Chen, *Adv. Mater.* **2017**, *29*, 1701410.

[4] W. Wan, C. A. Triana, J. Lan, J. Li, C. S. Allen, Y. Zhao, M. Iannuzzi, G. R. Patzke, *ACS Nano* **2020**, *14*, 13279.

[5] C. Si, Y. Zhang, C. Zhang, H. Gao, W. Ma, L. Lv, Z. Zhang, *Electrochim. Acta* **2017**, *245*, 829.

[6] Y. Fan, S. Ida, A. Staykov, T. Akbay, H. Hagiwara, J. Matsuda, K. Kaneko, T. Ishihara, *Small* **2017**, *13*, 1700099.

[7] C. Chen, D. Cheng, S. Liu, Z. Wang, M. Hu, K. Zhou, *Energy Storage Mater.* **2020**, *24*, 402.

[8] C. Chen, Y. Li, D. Cheng, H. He, K. Zhou, *ACS Appl. Mater. Interfaces* **2020**, *12*, 40415.

[9] M. Shen, C. Ruan, Y. Chen, C. Jiang, K. Ai, L. Lu, *ACS Appl. Mater. Interfaces* **2015**, *7*, 1207.

[10] L. Wei, L. Qiu, Y. Liu, J. Zhang, D. Yuan, L. Wang, *ACS Sustainable Chem. Eng.* **2019**, *7*, 14180.

[11] X. Feng, Q. Jiao, H. Cui, M. Yin, Q. Li, Y. Zhao, H. Li, W. Zhou, C. Feng, *ACS*

Appl. Mater. Interfaces **2018**, *10*, 29521.

[12] H.-F. Wang, C. Tang, B. Wang, B.-Q. Li, Q. Zhang, *Adv. Mater.* **2017**, *29*, 1702327.

[13] W. Fang, H. Hu, T. Jiang, G. Li, M. Wu, *Carbon* **2019**, *146*, 476.

[14] L. Ma, H. Zhou, Y. Sun, S. Xin, C. Xiao, A. Kumatani, T. Matsue, P. Zhang, S. Ding, F. Li, *Electrochim. Acta* **2017**, *252*, 338.

[15] X. Liu, L. Wang, P. Yu, C. Tian, F. Sun, J. Ma, W. Li and H. Fu, *Angew. Chem. Int. Ed.*, **2018**, *57*, 16166.

[16] G. Fu, Y. Liu, Y. Chen, Y. Tang, J. B. Goodenough and J. M. Lee, *Nanoscale*, **2018**, *10*, 19937.

[17] W. Liu, D. Zheng, L. Zhang, R. Yin, X. Xu, W. Shi, F. Wu, X. Cao and X. Lu, *Nanoscale*, **2021,***13*, 3019.

[18]X. Han, X. Ling, Y. Wang, T. Ma, C. Zhong, W. Hu and Y. Deng, *Angew. Chem. Int. Ed.* **2019**, *58*, 5359.

[19] Z. Wu, H. Wu, T. Niu, S. Wang, G. Fu, W. Jin and T. Ma, *ACS Sustain. Chem. Eng.*, **2020,** *8*, 9226.

[20] X. Han, X. Ling, D. Yu, D. Xie, L. Li, S. Peng, C. Zhong, N. Zhao, Y. Deng and W. Hu, *Adv. Mater.*, **2019**, *31*, 1905622.

[21] X. F. Lu, Y. Chen, S. Wang, S. Gao and X. W. Lou, *Adv. Mater.*, **2019**, *31*, 1902339.

[22] Q. Lu, J. Yu, X. Zou, K. Liao, P. Tan, W. Zhou, M. Ni and Z. Shao, *Adv. Funct. Mater.*, **2019**, *29*, 1904481.

[23] Z. Rong, C. Dong, S. Zhang, W. Dong and F. Huang, *Nanoscale*, **2020**, *12*, 6089.

[24] W. Liu, J. Zhang, Z. Bai, G. Jiang, M. Li, K. Feng, L. Yang, Y. Ding, T. Yu and Z. Chen, *Adv. Funct. Mater.*, **2018**, *28*, 1706675.